Solid State Ionics

Submitted 25 February 2014

(Revised) 8 April 2014

Synthesis and lithium-ion conductivity for perovskite-type $Li_{3/8}Sr_{7/16}Ta_{3/4}Zr_{1/4}O_3$ solid electrolyte by powder-bed sintering

Ryoji Inada*, Keisuke Kimura, Koji Kusakabe, Tomohiro Tojo, and Yoji Sakurai

Department of Electrical and Electronic Information Engineering, Toyohashi University of Technology, 1-1 Hibarigaoka, Tempaku-cho, Toyohashi, Aichi 441-8580, Japan.

*Corresponding author

Ryoji Inada, Associate Professor

Postal address: Toyohashi University of Technology, 1-1 Tempaku-cho, Toyohashi, Aichi 441-8580, Japan

Phone: +81-532-44-6723

Fax: +81-532-44-6757

E-mail address: inada@ee.tut.ac.jp

Abstract

Perovskite-type compounds ABO_3 in which A= La, Li and B = Ti ($Li_{2/3-3x}La_xTiO_3$, LLT) exhibit very high bulk ionic conductivity of 1.2×10^{-3} Scm^{-1} at 30°C, but LLT has very large grain-boundary resistance and is only stable above 1.6–1.8 V vs. Li/Li^+ because Ti^{4+} can be easily reduced to Ti^{3+} below this potential. $Li_{3/8}Sr_{7/16}Ta_{3/4}Zr_{1/4}O_3$ (LSTZ), in which A and B cations of $SrZrO_3$ are partially substituted by Li and Ta, has been reported to be more stable against the lithiated negative electrode than LLT. In this paper, we synthesized LSTZ by using "powder-bed sintering" method, which is commonly used for preparation of dense garnet-structured lithium-ion conductor $Li_7La_3Zr_2O_{12}$ (LLZ). At sintering process, the LSTZ pellet was covered with the same mother powder to suppress the excess Li loss during high temperature treatment and the formation of secondary phases. For LSTZ sintered with covering LSTZ mother powder, secondary phases such as $SrTa_2O_6$ and $Sr_2Ta_2O_7$ were significantly reduced and LSTZ grains in the pellet were in good contact with each other. According to these improvement, the bulk and total (bulk + grain-boundary) ionic conductivity at 27°C of LSTZ attained to 3.5×10^{-4} Scm^{-1} and 2.7×10^{-4} Scm^{-1}, respectively. The total conductivity at room temperature is approximately 3 times higher than that as previously reported and comparable with LLT and LLZ.

Keywords: perovskite, $Li_{3/8}Sr_{7/16}Ta_{3/4}Zr_{1/4}O_3$, solid electrolyte, powder-bed sintering, lithium ion conductivity

1. Introduction

All-solid-state lithium batteries are expected as one of the next generation energy storage devices because of their high energy density, high safety and excellent cycle stability [1, 2]. Development of solid inorganic lithium-ion conducting materials for the use as solid electrolyte is most important issue to realize all solid-state batteries. The materials used for solid electrolyte must have not only high lithium-ion conductivity σ_{Li} > 10^{-3} Scm^{-1} at room temperature but also chemical stability against metallic lithium or lithiated negative electrode, air and moisture. Although oxide based solid electrolyte materials have rather lower σ_{Li} than sulfide based one [1, 2], they have other advantages such as their chemical stability and easiness for handling.

Among the oxide lithium-ion conducting materials, perovskite-type $Li_{2/3-3x}La_xTiO_3$ (LLT) exhibits very high bulk ionic conductivity above 10^{-3} Scm^{-1} at room temperature [3–8]. However, its grain-boundary conductivity is limited only in the order of 10^{-5}–10^{-4} Scm^{-1} at room temperature [3–6], which results into much lower total (bulk + grain-boundary) conductivity than bulk one. Furthermore, its electronic conductivity could be increased substantially because the Ti^{4+} included in LLT is easily reduced to Ti^{3+} when LLT is in contact with metallic lithium or lithiated graphite inside a battery [7, 8]. It has been reported that the reduction from Ti^{4+} to Ti^{3+} in LLT is caused at the potential of 1.6–1.8 V vs. Li/Li^+ [7, 8]. This electrochemical stability window gives a great difficulty to use this material in a practical use for solid-state batteries.

Several papers for other perovskite-type lithium-ion conductor with higher stability than LLT have been reported [9–11]. Thangadurai et al. studied lithium-ion conductors $LiSr_{1.65}B_{1.3}B'_{1.7}O_9$ (B = Ti, Zr; B'= Nb, Ta) [9]. Although the Ti-contained materials have similar stability problem as in LLT, they suggested that $LiSr_{1.65}Zr_{1.3}Ta_{1.7}O_9$ is a

lithium-conductor with higher electrochemical stability than LLT. Although they did not show bulk and grain-boundary conductivity quantitatively, the total (bulk + grain boundary) ionic conductivity of $LiSr_{1.65}Zr_{1.3}Ta_{1.7}O_9$ was limited to 1.6×10^{-5} Scm^{-1} at 30°C. Watanabe et al. reported the properties of Ta containing $Li_{2x}Sr_{1-2x}M_{0.5-x}Ta_{0.5+x}O_3$ (M = Cr, Fe, Co, Al, Ga, In and Y) [10]. The bulk conductivity attained to 1×10^{-4} Scm^{-1} at 25°C when M = Fe and x = 0.25, but total conductivity is approximately two orders lower than bulk one due to the low sinterability. Chen et al. systematically investigated the crystal phase and ionic conductivity in $Li_{2x-y}Sr_{1-x}Ta_yZr_{1-y}O_3$ (y = 0.25−1, x = 3y/4) [11]. They reported that perovskite structure can be obtained at $y \leq 0.75$ and the highest bulk and total conductivities of 2.0×10^{-4} Scm^{-1} and 0.8×10^{-4} Scm^{-1} at 30°C in $Li_{3/8}Sr_{7/16}Ta_{3/4}Zr_{1/4}O_3$ (y = 0.75). In addition, this solid electrolyte is found to be stable at least above 1 V vs Li/Li^+, so that several anode materials operating at high potential for Li^+ storage such as $Li_4Ti_5O_{12}$, TiO_2 and Nb_2O_5 can be potentially used for constituting all-solid-state batteries. However, for applications to solid electrolyte, further reduction of the grain-boundary resistance in $Li_{3/8}Sr_{7/16}Zr_{3/4}Ta_{1/4}O_3$ by increasing sinterability and avoiding impurity phases should be necessary.

In this paper, we prepared perovskite-type $Li_{3/8}Sr_{7/16}Zr_{3/4}Ta_{1/4}O_3$ (LSTZ) by using powder-bed sintering method, which is commonly used to obtain dense garnet-structured $Li_7La_3Zr_2O_{12}$ (LLZ) and other related lithium-ion conductors [12–20]. The influence of sintering method on the crystal phases, microstructure and ionic conductivity of LSTZ were investigated.

2. Experimental

$Li_{3/8}Sr_{7/16}Zr_{3/4}Ta_{1/4}O_3$ (LSTZ) was prepared by a conventional solid state reaction

method. Stoichiometric amounts of Li_2CO_3 (Kojundo Chemical Laboratory Co., Ltd., 99.99%), $SrCO_3$ (Kojundo Chemical Laboratory Co., Ltd., 99.9%), ZrO_2 (Kojundo Chemical Laboratory Co., Ltd., 98%) and Ta_2O_5 (Kojundo Chemical Laboratory Co., Ltd., 99.9%) were ground and mixed in ethanol for 5 h by planetary ball-milling (Nagao System, Planet M2-3F) with zirconia ball, and then calcined at 1100°C for 12 h in alumina crucible. The calcined powders were ground again, and then pressed into pellets at the pressure of 300 MPa by cold isostatic pressing (CIP). Finally, the LSTZ pellets were sintered at 1300°C for 15 h in air using alumina crucible. The heat treatment temperature for LSTZ was referred to the condition reported in [11]. At sintering stage, the pellet was covered with or without the same mother powder to study the influence of sintering method on the properties of LSTZ. The quantity ration (wt%) of the pellet sample and mother powder was 1 : 2.

The crystal structure of the samples was evaluated by X-ray diffraction (XRD, Rigaku Multiflex) using CuKα radiation, with measurement range 2θ = 5–90° and step interval of 0.02°. Scanning electron microscope (SEM) and energy dispersive X-ray (EDX) analyses were performed using JSM-6300 (JEOL Ltd.) to investigate the fractured surface microstructure of the sintered pellet and the distribution of Sr, Ta and Zr elements. The composition of the elements in each sample was measured by inductively coupled plasma optical emission spectroscopy (ICP-OES).

Ionic conductivity was evaluated at temperature from 27 to 150°C and frequency from 5 Hz to 5 MHz with applied voltage amplitude of 0.1 V, using both Hioki Chemical Impedance Meter 3532-80 (for the measurement up to 1 MHz) and Hioki LCR Hightester 3532-50 (for the measurement from 1 MHz to 5 MHz). Electronic conductivity was evaluated at 30°C by potentiostatic polarization experiment, using a

battery test station TOYO System TOSCAT-3100 with an applied voltage of 4 V. Before the conductivity measurements, both parallel surfaces of the sintered pellet were sputtered with lithium-ion blocking Au electrodes.

3. Results and discussion

Sintered LSTZ pellets with or without mother powder were white color. XRD patterns of LSTZ samples sintered without or with mother powder are shown in Fig. 1. The main diffraction peaks for both samples belong to cubic perovskite structure. Minor peaks from secondary phases such as $SrTa_2O_6$ and $Sr_2Ta_2O_7$ are confirmed in LSTZ sintered without mother powder and $SrTa_2O_6$ and $LiTaO_3$ in LSTZ sintered with mother powder. The peak intensity of $SrTa_2O_6$ and $Sr_2Ta_2O_7$ in LSTZ sintered without mother powder is found to be much larger than in LSTZ sintered with mother powder. The elementary compositions evaluated by ICP-OES analysis for LSTZ samples with different sintering conditions are summarized in Table 1. It was clearly confirmed that Li content in LSTZ sintered without mother powders are significantly less than that sintered with mother powder. In addition, we also checked the composition of mother powder used for covering the pellet in sintering process, which is shown in Table 1. As well as the LSTZ pellet sintered without mother powder, it was confirmed that Li content maintained in the mother powder after sintering is much smaller than the pellet, which is due to the evaporation of Li during high temperature sintering. This result suggests that during high temperature sintering, Li loss in LSTZ is easily occurred and results into the formation of impurity phase such as $SrTa_2O_6$ and $Sr_2Ta_2O_7$. By covering the pellet with mother powder, both Li loss and the formation of impurity phase in pellet sample are suppressed remarkably. The obtained molar ratios of Sr, Ta and Zr in both

samples are nearly corresponding to nominal compositions. As shown in Fig. 1(b), very small amount of $SrTa_2O_6$ is still included in the sintered LSTZ with mother powder, which could be related with tiny Li deficiency in this sample. Although phase purity of sintered LSTZ could be improved further by adding appropriate excess lithium added in the starting materials, further investigation should be needed to examine the thermodynamical stability of the perovskite structure of LSTZ.

Fig. 2 shows fractured cross sectional SEM images for LSTZ samples with different sintering conditions. As can be seen, grain sizes in LSTZ sintered with mother powder are much larger than LSTZ sintered without mother powder. In LSTZ sintered with mother powder, grains with the size of 5–10 μm are in good contact with each other, while in LSTZ sintered without mother powder has rather porous structure and smaller grains with the size below 5 μm. This is attributed to the Li loss in LSTZ during high temperature sintering. By applying powder-bed sintering method, dense LSTZ with larger grains can be obtained. The density of each sintered pellet was determined from the weight and the physical dimensions. Measured density of LSTZ sintered with mother powder was estimated to be 5.80 gcm^{-3} and slightly higher than the density of LSTZ sintered without mother powder (= 5.67 gcm^{-3}). To examine further, we investigated the distribution of Sr, Ta and Zr in LSTZ pellet sintered without mother powder using EDX analysis. The results are shown in Fig. 3. As can be seen, the distributions for Sr and Ta are nearly identical. The distribution for Zr also seems to be similar with that for Sr or Ta. However, the presence of Zr cannot be confirmed clearly at the left part of the grain positioned near the center of observed area (marked with dotted lines), indicating that $SrTa_2O_6$ or $Sr_2Ta_2O_7$ without including Zr is formed on the surface of LSTZ grain. During high temperature sintering, Li evaporation is expected to

be caused on the surface of LSTZ grains. After Li evaporation, $SrTa_2O_6$ or $Sr_2Ta_2O_7$ could be formed on the grain surface or grain boundary, which inhibits the sintering process and grain growth. Therefore, small grains and pores are observed in the pellet sintered without mother powder (Fig. 2(a)). Such difference in microstructure and content of secondary phases among the sample strongly influences on the lithium-ion conduction particularly at grain-boundary.

The conductivity of LSTZ with different sintering conditions was examined by AC impedance spectroscopy using Au electrodes. Fig. 4 shows typical impedance plots measured at room temperature (27°C) for LSTZ. For direct comparison among the samples with different geometrical sizes, real and imaginary parts of impedance Z and Z" multiplied by a factor of A/L are plotted in Fig. 4, where A and L are surface area and thickness of each pellet. For both LSTZ samples, semicircle(s) and linear portion data were obtained in high and low frequency regions, indicating that the conducting nature is primary ionic. Intercept point of linear tail in low frequency range with real axis nearly corresponds total (bulk and grain-boundary) resistance R_{total}. As shown in Fig. 3(a), only one distorted semicircle was confirmed in impedance plot for LSTZ sintered without mother powder. On the other hand, as shown in Fig. 3(b), the plot could be well resolved into bulk and grain-boundary resistances, R_{Bulk} and R_{GB}. $R_{total} = R_{Bulk} + R_{GB}$ in LSTZ sintered without mother powder is 6 times larger than LSTZ sintered with mother powder. Since the difference in bulk conductivity is expected to be small among the both LSTZ samples, R_{GB} in LSTZ sintered without mother powder is considerably larger than LSTZ sintered with mother powder. This is attributed to smaller size and their weak connectivity of LSTZ grains by secondary phases such as $SrTa_2O_6$ and $Sr_2Ta_2O_7$ formed on the LSTZ grain surface or grain boundary by Li evaporation, as

shown in Figs. 2 and 3.

Total conductivity σ for each LSTZ sample can be calculated by the inverse of R_{total} and geometrical parameter of the sample. The values of σ at 27°C for all sample calculated from the data in Fig. 4 are summarized in Table 2. σ for LSTZ sintered with same mother powder is estimated to be 2.7×10^{-4} Scm^{-1}, which is 6 times higher than LSTZ sintered without mother powder ($\sigma = 0.4 \times 10^{-4}$ Scm^{-1}). This is mainly attributed to both avoidance of impurity phases (Fig. 1) and larger LSTZ grains connected well with each other (Fig. 2) in LSTZ sintered with mother powders. In addition, σ of present LSTZ sintered with mother powder is approximately 3 times higher than the value as previously reported ($\sigma = 0.8 \times 10^{-4}$ Scm^{-1}) [11], and comparable with dense LLT with much higher bulk conductivity above 10^{-3} Scm^{-1} [6]. For LSTZ sintered with mother powders, semicircles due to ionic conduction in bulk (at higher frequency region) and grain-boundary (at lower frequency region) were clearly separated, so that bulk conductivity σ_{Bulk} of LSTZ can be determined quantitatively. As a result, σ_{Bulk} of LSTZ was estimated to be 3.5×10^{-4} Scm^{-1}, which is 1.8 times higher than the value as previously reported ($\sigma_{Bulk} = 2.0 \times 10^{-4}$ Scm^{-1}) [11]. Potentiostatic polarization measurements of LSTZ sample sintered with mother powder were made to investigate the electron conduction contribution. Since we used the lithium-ion blocking Au electrodes for the measurement, the steady state current of current-time profile shown in Fig. 5 is attributed to electronic conduction in LSTZ sample. Electronic conductivity σ_e can be determined from applied DC voltage (= 4 V), steady state current (= 0.284 μA) and geometrical parameters (surface area and thickness) of LSTZ pellet sample. It is confirmed that σ_e is approximately 4 orders of magnitude lower than the ionic one

(Table 2), which demonstrates the dominant lithium-ion conduction of LSTZ.

Temperature dependence of total conductivity σ for both LSTZ samples was also measured in the temperature range from 27 to 150°C. Fig. 6 shows variation of the total conductivity σ for LSTZ as a function of inverse of temperature 1000/*T*. LSTZ sintered with same mother powder has higher σ than LSTZ sintered without same mother powder. The temperature dependence of σ is well expressed by the Arrhenius equation $\sigma T = \sigma_0 \exp(-E_a / k_B T)$. Here, σ_0 is constant, E_a is activation energy of conductivity and k_B is Boltzmann constant (= 1.381×10^{-23} J/K), respectively. As shown in (1), E_a of each sample can be estimated from the slope of σT data plotted in Fig. 5. As summarized in Table 2, E_a of LSTZ sintered with same mother powder is estimated as 0.36 eV, while LSTZ sintered without mother powder has higher E_a (= 0.40 eV). This is mainly attributed to the difference in lithium ion conduction of LSTZ grain boundaries among both samples. As shown in Fig. 3, grain boundary resistance of LSTZ sintered without same mother powder is much larger than LSTZ sintered with same mother powder, which is due to smaller size and their weak connectivity of LSTZ grains by secondary phases such as $SrTa_2O_6$ and $Sr_2Ta_2O_7$ formed on the LSTZ grain surface or grain boundary by Li evaporation, as shown in Figs. 2 and 3.

At present, impurity phases are not avoided completely in LSTZ by powder-bed sintering, so that there is the room for further improvement in the ionic conductivity. Appropriate excess lithium can be added in the starting materials to optimize the phase purity and the conductivity of the LSTZ. Moreover, detailed examination of crystal structure for LSTZ should be needed to clarify its good ionic conduction property.

4. Conclusion

We synthesized perovskite type $Li_{3/8}Sr_{7/16}Ta_{3/4}Zr_{1/4}O_3$ (LSTZ) solid electrolyte by using powder-bed sintering method, which is commonly used for preparation of dense garnet-structured $Li_7La_3Zr_2O_{12}$ (LLZ). At sintering process, the LSTZ pellet was covered with the same mother powder to suppress the excess Li loss during high temperature treatment. By sintering LSTZ pellet with same mother powder, secondary phases such as $SrTa_2O_6$ and $Sr_2Zr_2O_7$ were greatly reduced and larger LSTZ grains in the pellet were in good contact with each other. The bulk and total ionic conductivity at 27°C in LSTZ sintered with same mother powder attained to 3.5×10^{-4} S cm^{-1} and 2.7×10^{-4} S cm^{-1}, respectively. The total conductivity at room temperature is approximately 3 times higher than that as previously reported and nearly comparable with perovskite-type $Li_{2/3-3x}La_xTiO_3$ with much higher bulk ionic conductivity than LSTZ.

Acknowledgments

This work was partly supported by JSPS KAKENHI Grant Number 26630111 and Research Foundation for the Electrotechnology of Chubu (R-25209).

References

[1] K. Takada, Acta Mater. 61 (2013) 759–770.

[2] M. Tatsumisago, M. Nagao, A. Hayashi, J. Asian Ceram. Soc. 1 (2013) 17–25.

[3] Y. Inaguma, C. Liquan, M. Itoh, T. Nakamura, Solid State Commun. 86 (1993) 689–693.

[4] Y. Harada, H. Watanabe, J. Kuwano, Y. Saito, J. Power Sources. 81–82 (1999) 777–781.

[5] C.W. Ban, G.M. Choi, Solid State Ionics 140 (2001). 285–292.

[6] Y. Inaguma, M Nakashima, J. Power Sources 228 (2013) 250–255.

[7] C.H. Chen, K. Amine, Solid State Ionics 144 (2001) 51–57.

[8] C. Hua, X. Fang, Z. Wang, L. Chen, Electrochem. Commun. 32 (2013) 5–8.

[9] V. Thangadurai, A.K. Shukla, J. Gopalakrishnan, Chem. Mater. 11 (1999) 835–839.

[10] H. Watanabe, J. Kuwano, J. Power Sources 68 (1997) 421–426.

[11] C.H. Chen, S. Xie, E. Sperling, A.S. Yang, G. Henriksen, K. Amine, Solid State Ionics 167 (2004) 263–272.

[12] R. Murugan, V. Thangadurai, W. Weppner, Angew. Chem. Int. Ed. 46 (2007) 7778–7781.

[13] S. Kumazaki, Y. Iriyama, K.H. Kim, R. Murugan, K. Tanabe, K. Yamamoto, T. Hirayama, Z. Ogumi, Electrochem. Commun. 13 (2011) 509–512.

[14] Y. Li, J. Han, C. Wang, S. C. Vogel, H. Xie, M. Xu, J.B. Goodenough, J. Power Sources 209 (2012) 278–281.

[15] R. Murugan, S. Ramakumar, N. Janani, Electrochem. Commun. 13 (2011) 1373–1375.

[16] S. Kumazaki, Y. Iriyama, K-H. Kim, R. Murugan, K. Tanabe, K. Yamamoto, T. Hirayama, Z. Ogumi, Electrochem. Commun. 13 (2011) 509–512.

[17] Y. Shimonishi, A. Toda, T. Zhang, A. Hirano, N. Imanishi, O. Yamamoto, Y. Takeda, Solid State Ionics 183 (2011) 48–53.

[18] S. Ohta, T. Kobayashi, T. Asaoka, J. Power Sources 196 (2011) 3342–3345.

[19] Y. Li, J. Han, C. Wang, H. Xie, J.B. Goodenough, J. Mater. Chem. 22 (2012) 15357–15361.

[20] R. Inada, K. Kusakabe, T. Tanaka, S. Kudo, Y. Sakurai, Solid State Ionics, in press. http://dx.doi.org/10.1016/j.ssi.2013.09.008

Table 1. Elementary composition of LSTZ with different sintering conditions estimated from ICP-OES analysis. The data for mother powder used for covering the pellet in sintering process was also shown. Note that Zr content is fixed at 0.25 for calculation the content of each element.

Element in LSTZ (Nominal composition)	Li (0.375)	Sr (0.4375)	Ta (0.75)	Zr (0.25)
Sintered pellet without mother powder	0.325	0.452	0.804	0.250
Sintered pellet with mother powder	0.372	0.443	0.789	0.250
Mother powder used for covering the pellet in sintering process	0.333	0.438	0.874	0.250

Table 2. Summary of bulk ionic conductivity σ_{Bulk}, total (bulk + grain boundary) conductivity σ, activation energy E_a for σ, and electronic conductivity σ_e for LSTZ with different sintering conditions.

Sintering condition	Bulk ionic conductivity at 27°C σ_{Bulk} / S cm^{-1}	Total ionic conductivity at 27°C σ / S cm^{-1}	Activation energy of σ E_a / eV	Electronic conductivity at 30°C σ_e / S cm^{-1}
Sintered without mother powder	–	0.44×10^{-4}	0.40	–
Sintered with mother powder	3.5×10^{-4}	2.7×10^{-4}	0.36	2.1×10^{-8}

Figure captions

Fig. 1. XRD patterns of LSTZ with different sintering conditions: (a) sintered without mother powders and (b) sintered with mother powders.

Fig. 2. SEM images of the fractured cross section for LSTZ with different sintering conditions: (a) sintered without mother powders and (b) sintered with mother powders.

Fig. 3. SEM image for LSTZ sintered without mother powders (a) and corresponding elementary mapping of Sr (b), Ta (c) and Zr (d) obtained from EDX analysis.

Fig. 4. AC impedance plot obtained at 27°C for LSTZ sintered without mother powders and (a) and with mother powders (b).

Fig. 5. Potentiostatic polarization current as a function of measuring time at 30°C for LSTZ sintered with mother powders using lithium-ion blocking Au electrodes.

Fig. 6. Arrhenius plots for total (bulk + grain-boundary) ionic conductivity σ for LSTZ with different sintering conditions.

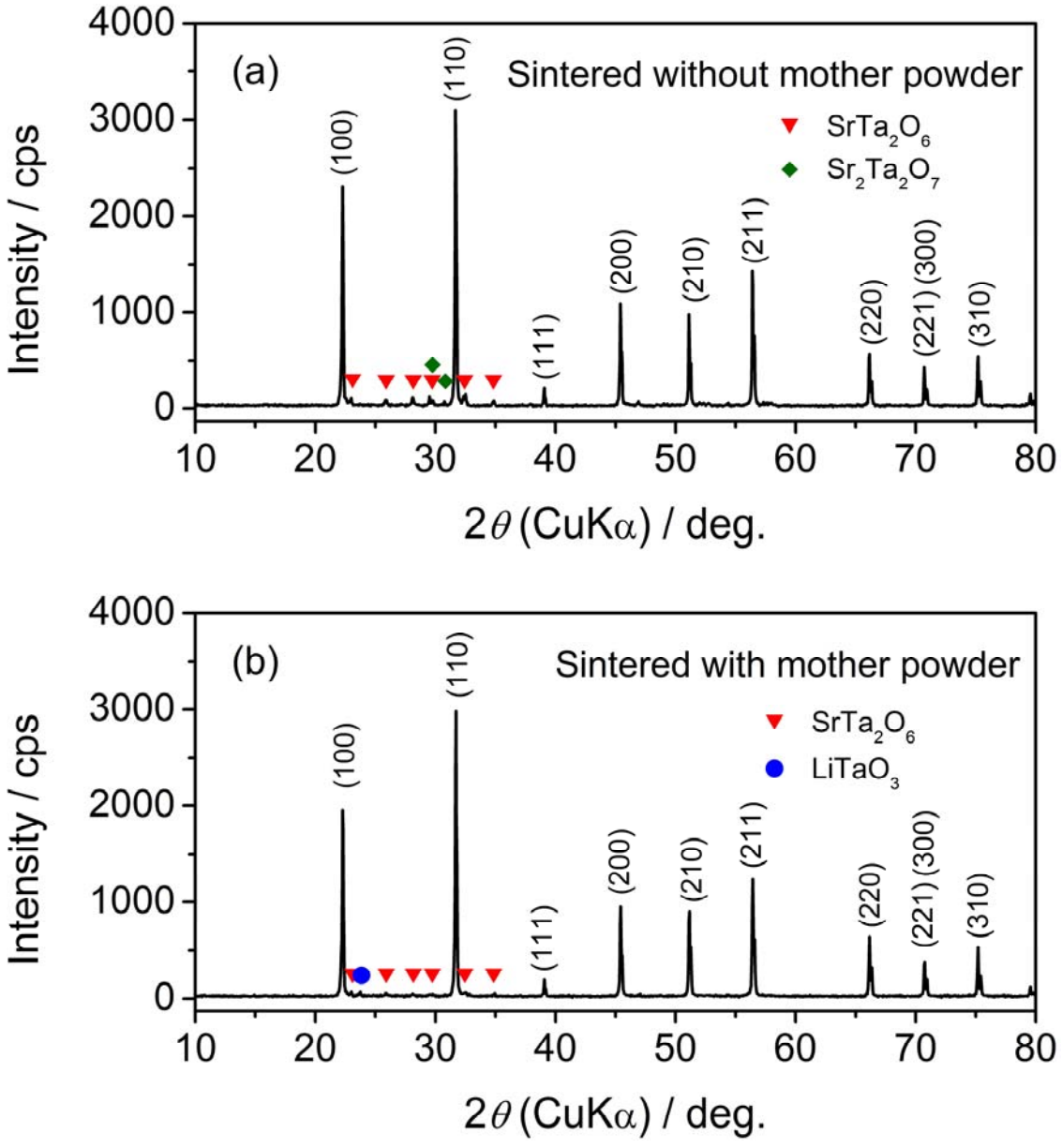
(a)
Sintered without mother powder
SrTa2O6
Sr2Ta2O7
(100)
(110)
(111)
(200)
(210)
(211)
(220)
(221) (300)
(310)
Intensity / cps
2θ (CuKα) / deg.
(b)
Sintered with mother powder
SrTa2O6
LiTaO3
(100)
(110)
(111)
(200)
(210)
(211)
(220)
(221) (300)
(310)
Intensity / cps
2θ (CuKα) / deg.

Fig. 1

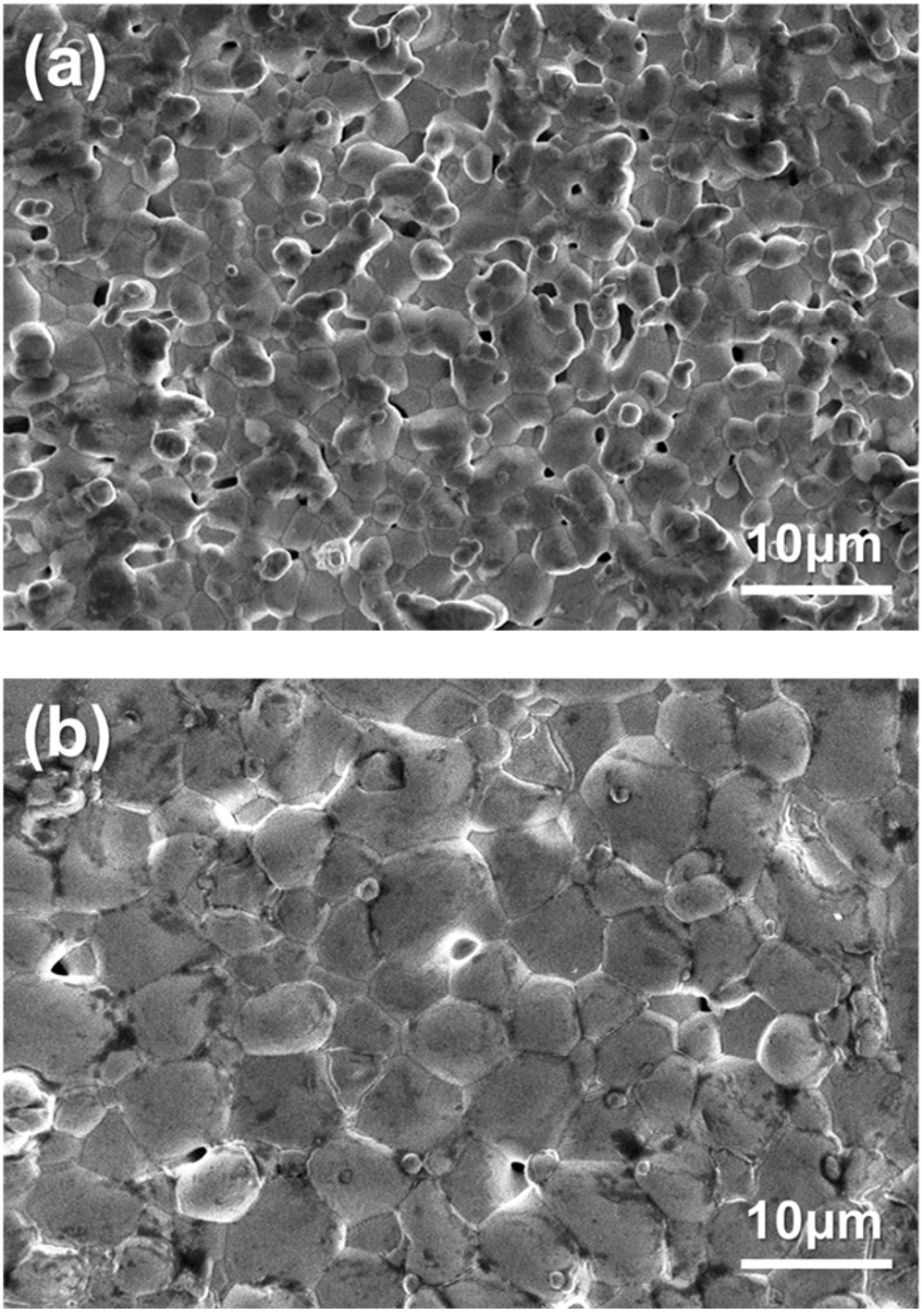

Fig. 2

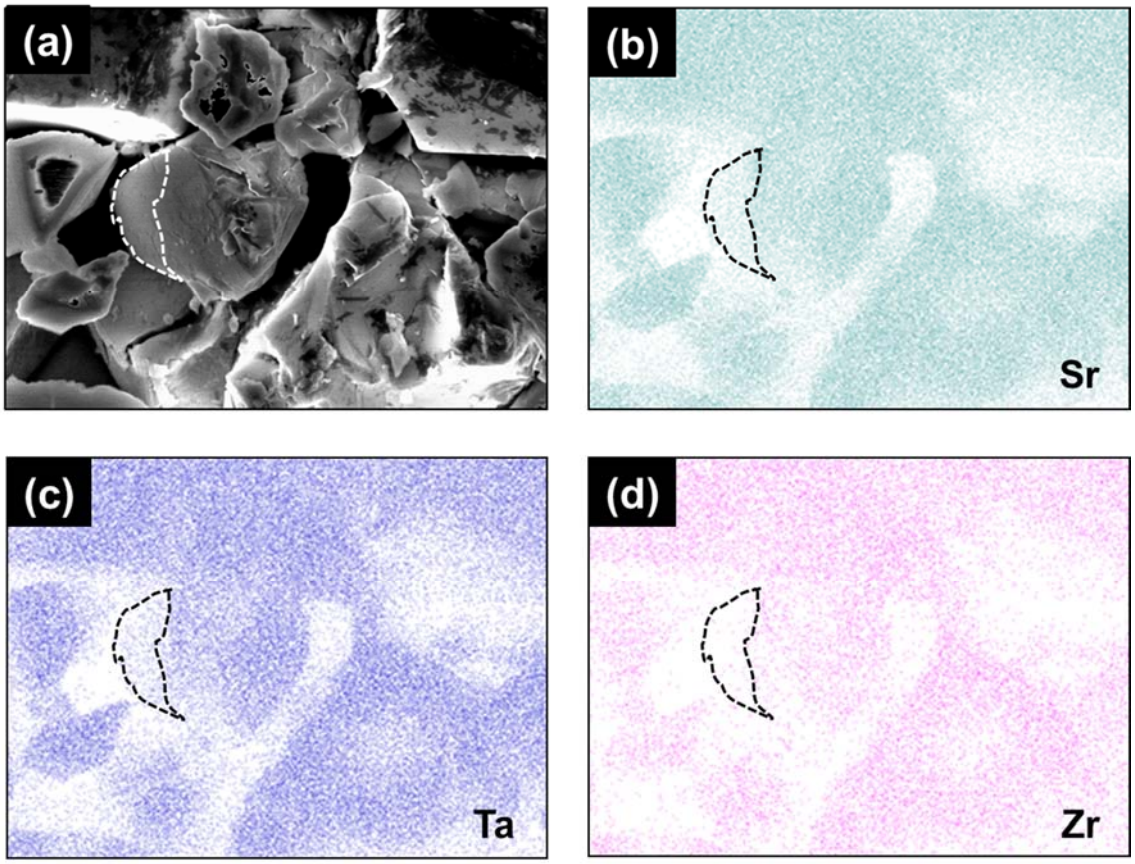

Fig. 3

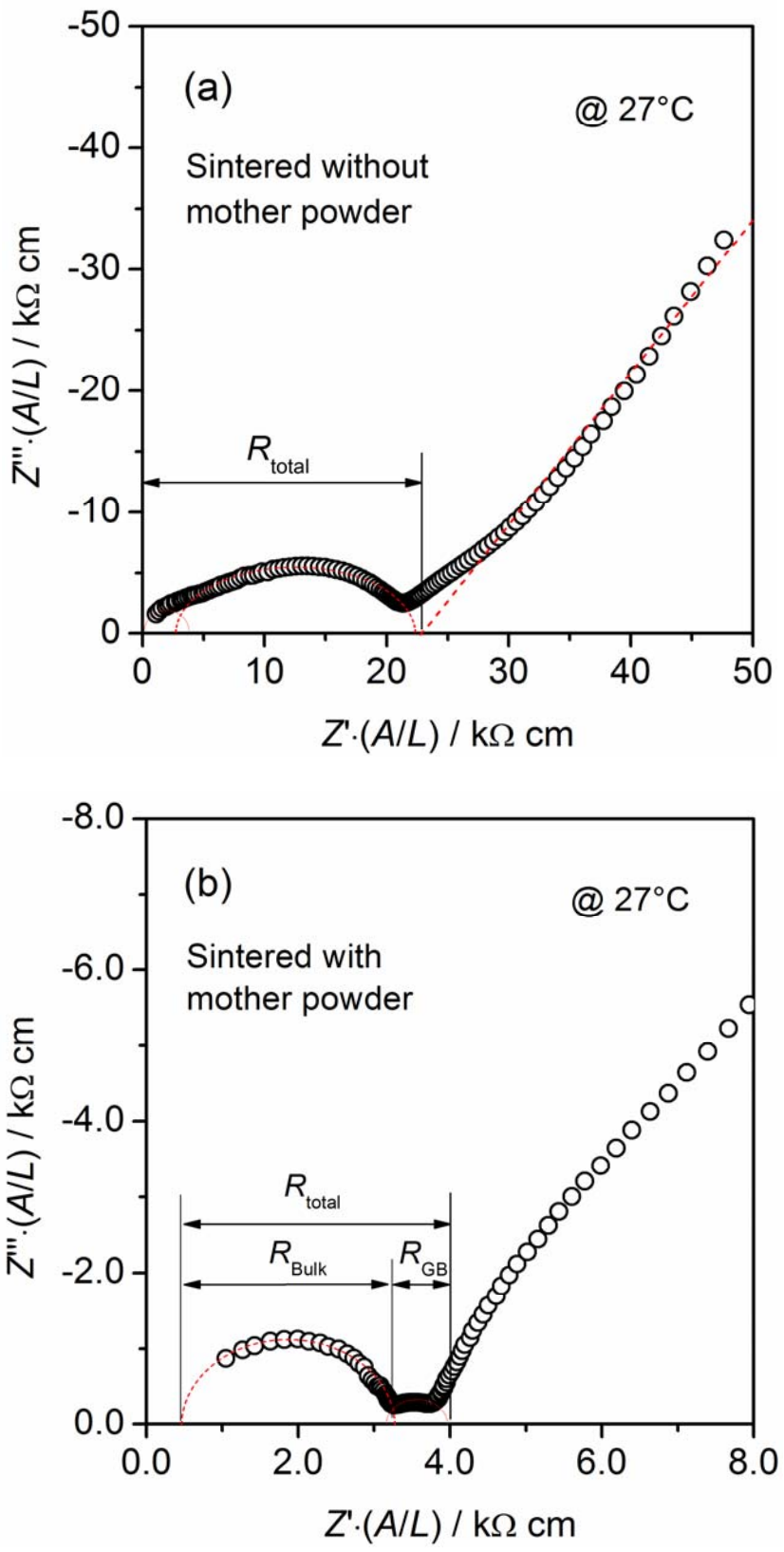
(a)
@ 27°C
Sintered without
mother powder
R_{total}
Z''·(A/L) / kΩ cm
Z'·(A/L) / kΩ cm
-50
-40
-30
-20
-10
0
0
10
20
30
40
50
(b)
@ 27°C
Sintered with
mother powder
R_{total}
R_{Bulk}
R_{GB}
Z''·(A/L) / kΩ cm
Z'·(A/L) / kΩ cm
-8.0
-6.0
-4.0
-2.0
0.0
0.0
2.0
4.0
6.0
8.0

Fig. 4

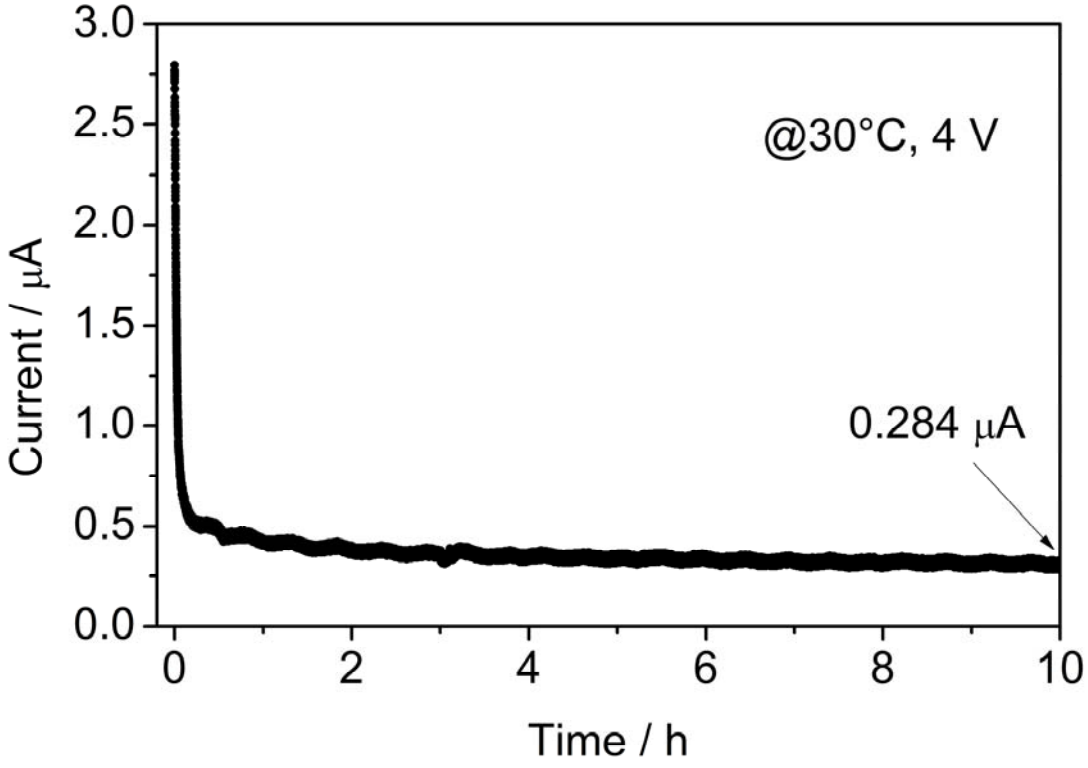

Fig. 5

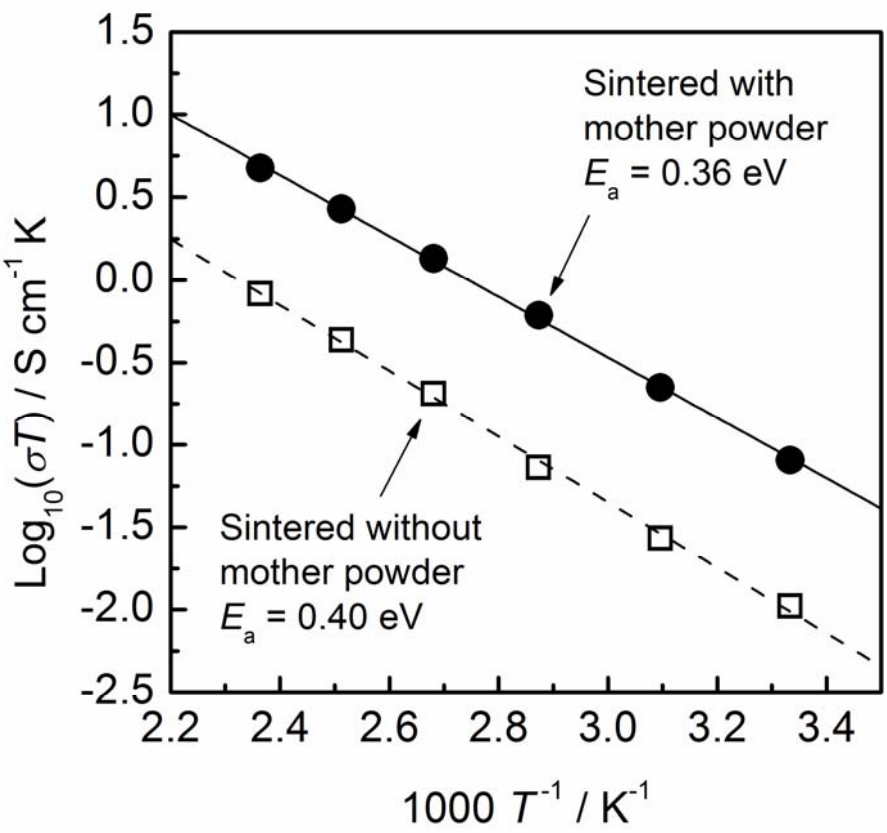
Sintered with
mother powder
E_a = 0.36 eV
Sintered without
mother powder
E_a = 0.40 eV
$\mathrm{Log_{10}}(\sigma T)$ / S cm^{-1} K
1000 T^{-1} / K^{-1}
1.5
1.0
0.5
0.0
-0.5
-1.0
-1.5
-2.0
-2.5
2.2
2.4
2.6
2.8
3.0
3.2
3.4

Fig. 6